Electronic structure of RuS_2

N. A. W. Holzwarth
Department of Physics, Wake Forest University, Winston-Salem, North Carolina 27109

Suzanne Harris and K. S. Liang
Corporate Research Science Laboratories, Exxon Research and Engineering Company, Route 22 East, Annandale, New Jersey 08801

(Received 10 May 1985)

The electronic structure of the pyrite material RuS_2 was investigated with use of self-consistent band-structure calculations and x-ray photoemission experiments. Short-range interactions are found to determine the grouping of bands, consistent with molecular-orbital and crystal-field analyses discussed in the literature for the related material FeS_2. The occupied bands have small dispersion. However, the bottom of the first conduction band at the center of the Brillouin zone is found to have appreciable dispersion as characterized by an effective mass of approximately $0.5m_e$.

I. INTRODUCTION

RuS_2 is an interesting material from both a fundamental and a technological point of view. It is one of the semiconducting transition-metal—dichalcogenide materials having the pyrite structure.[1] It has possible uses as a catalyst[2] and as a photoelectrode.[3]

In this paper, we present a detailed study[4] of the electronic structure of RuS_2, including the results of x-ray photoemission experiments and the results of first-principles, self-consistent band-structure calculations. We find our results to be consistent with electrical and optical properties reported in the literature.[3,5]

It has been the goal of several researchers[6] to understand the systematic trends of the transition-metal—dichalcogenide materials throughout the Periodic Table. Many of these materials exhibit unusual electronic properties including ferromagnetism and antiferromagnetism, metal-nonmetal transitions, structural instabilities, charge-density waves, and superconductivity. These materials exist in a few well-defined structural forms—layered forms including both octahedral and trigonal prismatic coordination of the transition metals, and nonlayered forms including pyrite and marcasite structures. It is not surprising that the electronic structure of these materials are to a first approximation very similar—having chalcogen p-band widths of roughly 5 eV, narrow crystal-field split transition metal d bands, and weak hybridization between these bands. For given structural forms, rigid-band models have gone a long way toward understanding trends across a row of the Periodic Table. Therefore, we attempt to place our results for RuS_2 into context with respect to other transition-metal —dichalcogenide materials.

The outline of the paper is as follows. In Sec. II, the calculational and experimental methods are described. In Sec. III, we present the results of our detailed band-structure calculations for RuS_2 in its pyrite structure. Also presented are the results of the experimental photoemission measurements which are compared with the calculated densities of states. Our work is summarized and concluded in Sec. IV.

II. METHODS

A. Calculational

Self-consistent, first-principles band-structure calculations were carried out within density-functional theory[7] in the local-density approximation,[8] using numerical techniques based on the treatment of the electron-ion interaction in the pseudopotential approximation.[9] The exchange-correlation potential was approximated using the form of Hedin and Lundqvist.[8]

First-principles, norm-conserving pseudopotentials for Ru and S were generated according to the scheme of Kerker,[10] using the matching radii listed in Table I. For Ru, relativistic effects other than the spin-orbit interaction were taken into account, using the Dirac equation to construct the spin-averaged pseudopotential in the manner similar to that of Kleinman[11] and of Bachelet and Schluter.[12] Neglect of the spin-orbit interaction of Ru was justified by considering that for atomic Ru, the spin-orbit splitting of the $4d$ level is approximately 0.3 eV, considerably smaller than the crystal-field splittings and bandwidths in RuS_2. For S, relatively large matching radii were chosen for the s and p pseudopotentials to ensure that S contributions to the wave functions in RuS_2 could be adequately represented by a plane-wave expansion. For the S potential, d wave and higher angular momenta interactions were approximated by the p-wave pseudopotential; for the Ru potential, f wave and higher angular momenta interactions were approximated by the d-wave pseudopotential. These angular approximations are expected to be entirely adequate for the valence bands and first set of conduction bands of RuS_2, but may introduce errors in the higher conduction bands.

The electronic wave functions were represented in terms of a mixed basis set consisting of plane waves and linear combinations of atomic orbitals (LCAO's) as developed by Louie, Ho, and Cohen.[9] The atomic orbitals were taken to be the numerical d-wave atomic pseudo wave functions

TABLE I. Numerical parameters used for bulk band calculations.

Pseudopotential parameters[a]	
Ru	$r_s=2.5$ bohr
	$r_p=3.0$
	$r_d=2.0$
S	$r_s=1.8$ bohr
	$r_p=2.2$
Mixed basis parameters[b]	
Plane-wave expansion	$\lvert k+G\rvert^2 \lesssim 7$ bohr^{-2}
Expansion of LCAO functions (Ru d wave functions)	$\lvert k+G\rvert^2 \lesssim 49$ bohr^{-2}

[a]Reference 10. [b]Reference 9.

for Ru. The truncation of the plane-wave basis expansion and of the plane-wave expansion of the LCAO matrix elements used in the present calculation is listed in Table I. For this choice of truncation, the eigenvalues of the occupied states and first few excited states are expected to be converged to better than 0.3 eV.

The matrix elements of the Hamiltonian involving the nonlocal (l-dependent) contributions to the pseudopotential were evaluated by using a separable form approximation similar to that used in previous electronic structure calculations.[13] In the present work, the radial portion of the nonlocal pseudopotential was fitted to a sum of Gaussian functions. The plane-wave matrix elements for these Gaussian functions could be evaluated analytically in terms of modified Bessel functions. By making power-series expansions of the modified Bessel functions, a separable form for the plane-wave matrix elements of the nonlocal potential could be obtained. This form is necessary for efficient evaluation of the matrix elements of the nonlocal potential between LCAO basis functions.

The densities of states were estimated according to the formula

$$n(E)\equiv\sum_n\int_{BZ}d^3k\,\delta(E_n(\mathbf{k})-E)$$
$$\approx\sum_i w_i\sum_n f(E_n(\mathbf{k}_i)-E)\,, \qquad (1)$$

where

$$f(x)\equiv\frac{1}{\Delta}\left[\frac{e^{x/\Delta}}{(1+e^{x/\Delta})^2}\right].$$

Here the integral over the Brillouin zone was approximated by a discrete sum over $\mathbf{k}$ points $\mathbf{k}_i$ with weight factors w_i. The discrete points were chosen by means of a midpoint algorithm with a uniform grid in order to perform the sum; 11 $\mathbf{k}$ points within the irreducible sector ($\frac{1}{24}$th) of the Brillioun zone were used. $E_n(\mathbf{k})$ denotes the band energy of the nth band at wave vector $\mathbf{k}$. The delta function $\delta(E-E_n(\mathbf{k}))$ was replaced by the function $f(x)$ which was taken to be the negative of the derivative of the Fermi function, using the smoothing parameter $\Delta=0.15$ eV. This method provides qualitative results for the densities of states; because of the use of the smoothing function $f(x)$, details of the band edges cannot be well represented by this method. Partial densities of states were evaluated in a similar way by multiplying Eq. (1) by an additional weight factor for each state equal to its charge density integrated within spheres centered on the S and Ru atoms.

B. Experimental

The photoemission measurements were performed on polycrystalline RuS_2 powder. The sample was prepared by the reaction of ammonium hexachlororuthenate with H_2S, followed by high-temperature annealing.[14] A pressed pellet of the powder was then used for the study. Before measurement, the surface of the pellet was treated using a gas mixture of 15 vol% H_2S and 85 vol% H_2 at 200 °C for about 1 h. This effectively removed the surface oxide. The gas treatment was performed in a preparation chamber attached to a Leybold-Heraeus LHS-10 spectrometer as previously described.[15] The x-ray photoemission (XPS) measurements were performed in the analysis chamber which maintained a base pressure of approximately 1.2×10^{-10} Torr. The x-ray source was Mg $K\alpha$ (1253.6 eV).

III. ELECTRONIC STRUCTURE OF RuS_2

A. Pyrite crystal structure

Naturally occurring RuS_2 (the mineral laurite) and annealed synthetic RuS_2 have the pyrite crystal structure, having the space-group symmetry[16] $T_h^6(Pa^3)$ with four RuS_2 groups per unit cell as summarized in Table II. The lattice parameters for RuS_2 were determined by Sutarno, Knop, and Reid[1] and are listed in Table II. The pyrite structure differs from many of the other structural forms of transition metal dichalcogenides by the presence of paired S sites separated by distance close to the bond length of a S_2 molecule. The pyrite structure is best described as a modified NaCl structure with two interpenetrating fcc sublattices. Ru atoms are located on one fcc sublattice and S_2 molecules are located on the other. The S_2 molecules orient themselves along four equivalent (111) directions so that the Ru atoms are in a nearly octahedral environment, surrounded by six nearest-neighbor S atoms. The S atoms are located in nearly tetrahedral sites surrounded by three nearest-neighbor Ru atoms and one nearest-neighbor S atom. The deviation from octahedral and tetrahedral geometry depends upon the ratio of the S—S bond length b to the cubic lattice constant a as parametrized by the positional parameter v, according to the relations listed in Table II. The parameter v is defined by $b/a=2\sqrt{3}v$. A value of v approximately equal to 0.09 yields the minimal distortion from octahedral and tetrahedral geometry. For most known pyrites, v ranges from 0.10 to 0.13,[17] RuS_2 having a value of 0.1121.[1] This means that the Ru site has a small trigonal distortion such that S—Ru—S bond angles in planes not containing the trigonal axis are slightly dilated at 94.1° and S—Ru—S bond angles in planes containing the trigonal axis are

TABLE II. Geometrical parameters for RuS_2.

	For general pyrite material MX_2	For RuS_2
Space group[a]	T_h^6	T_h^6
Cubic lattice constant	a	5.6095 Å[b]
Atomic positions	M (000),$(0\frac{1}{2}\frac{1}{2})$ $(\frac{1}{2}0\frac{1}{2}),(\frac{1}{2}\frac{1}{2}0)$	
	X $\pm(\frac{1}{2}-u,\frac{1}{2}-u,\frac{1}{2}-u)$ $\pm(u,-u,\frac{1}{2}-u)$ $\pm(\frac{1}{2}-u,u,-u)$ $\pm(-u,\frac{1}{2}-u,u)$	$u=0.1121$[b]
Bond lengths	$d_{M-X}=a(3u^2-u+\frac{1}{4})^{1/2}$	2.351 Å[b]
	$d_{X-X}=2\sqrt{3}au$	2.179 Å[b]
Bond angles	$\angle X-M-X=90°+\epsilon$	$\epsilon=4.1°$[b]
	$\epsilon=\sin^{-1}\left[\frac{u^2}{3u^2-u+\frac{1}{4}}\right]$ ($\epsilon=0$ for octahedral geometry)	
	$\angle X-X-M=\cos^{-1}\left[\frac{3u-\frac{1}{2}}{\sqrt{3}(3u^2-u+\frac{1}{4})^{1/2}}\right]$	103.2°[b]
	$\angle M-X-M=\cos^{-1}\left[\frac{3u^2-u}{3u^2-u+\frac{1}{4}}\right]$ (angle 109.5° for tetrahedral geometry)	115.0°[b]

[a]Reference 16.
[b]Reference 1.

slightly contracted at 85.9°. Also the S site is distorted from tetrahedral symmetry so that the three Ru—S—Ru bonds are dilated to 115.0° (compared to the tetrahedral angle of 109.5°) while the Ru—S—S bond is contracted to 103.2°.

B. Calculated energy bands of RuS_2

The self-consistent energy-band structure of pyrite RuS_2 is presented in two figures. In Fig. 1, the full valence-band structure is presented in comparison with a hypothetical S material in order to discuss qualitative aspects of the bonding. In Fig. 3, a portion of the band structure is presented in greater detail with symmetry labels in order to discuss electrical and optical properties. In these figures (as well as throughout this paper), the zero of energy is placed at the highest occupied energy.

1. Local bonding

Figure 1(a) shows the full valence-band structure of pyrite RuS_2. From this figure, one can see that there are five groups of bands which we will label I—V in order of increasing energy. This group reflects the fact that the energy bands of RuS_2 are dominated by short-range interactions, as discussed in the literature.[18,19] To a first approximation, the short-range interactions can be described in terms of states derived from S_2 molecular orbitals together with states derived from Ru $4d$ atomic orbitals, split by an octahedral crystal field. Since there are four RuS_2 units in each unit cell, the occupied bands must accommodate 80 valence electrons. Hence, there are 40 occupied valence bands for this material. States derived from the S_2 molecular orbitals alone are shown in Fig. 1(b) in terms of the bands of a hypothetical material (labeled S_2^{2-}) having the same structure except that the Ru^{+2} ions have been removed. These states correspond to those of a homonuclear diatomic molecule—(in order of

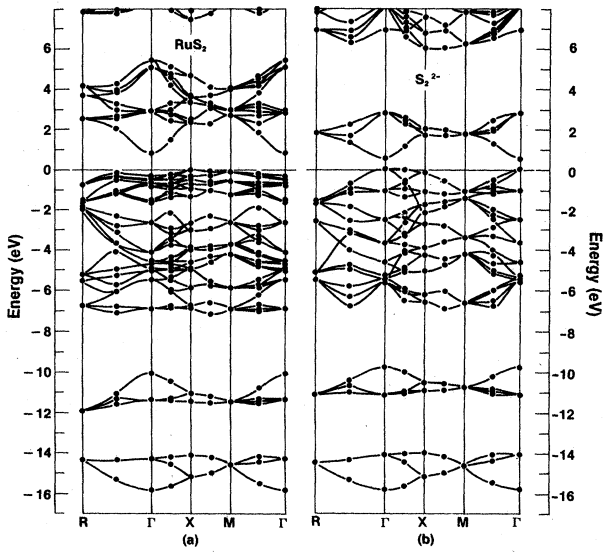

FIG. 1. Energy-band diagram for pyrite RuS_2 (a) and for hypothetical ionic S_2^{2-} in the pyrite structure. Zero of energy chosen at highest occupied level.

increasing energy) $3s\sigma$, $3s\sigma^*$, $3p\sigma$, $3p\pi$, $3p\pi^*$, and $3p\sigma^*$. The S $3s\sigma$ and σ^* states form two sets of four narrow bands centered at -14.6 and -10.8 eV, respectively. For future reference, we will label these two groups of bands I and II, respectively. The placement of these bands, their dispersion, and also their charge density is nearly identical in the hypothetical S_2^{2-} material and in RuS_2.

The S $3p$ states are split into two groups of bands in the hypothetical S_2^{2-} material. The lower group of 20 bands having a minimum energy of approximately -7 eV is completely occupied and can be associated with the $3p\sigma$, $3p\pi$, and $3p\pi^*$ molecular orbitals of S_2^{2-}. The higher group of four bands, associated with the $3p\sigma^*$ molecular orbital, are completely unoccupied, being separated from the occupied bands by a minimum band gap of 0.5 eV in the hypothetical S_2^{2-} compound. The basic structure of the S $3p$ states of S_2^{2-} is present in RuS_2 together with additional structure due to hybridization with the Ru $4d$ levels. The Ru atoms in RuS_2 are located in a nearly octahedral environment due to the Ru-S bonds. In an octahedral field, five-fold degenerate $4d$ atomic orbitals are split into three-fold degenerate t_{2g} orbitals and two-fold degenerate e_g orbitals. The t_{2g} orbitals orient themselves away from the Ru—S bonding directions and are essentially nonbonding. These levels form a group of 12 narrow bands (of total width 1.6 eV) just below the Fermi level. The e_g orbitals, on the other hand, orient themselves along the Ru—S bonding directions and hybridize with the S $3p$ levels. This hybridization occurs in such a way as to preserve the level structure of the S $3p$ bands of the hypothetical S_2^{2-} material. The bonding Ru e_g—S $3p$ hybrid states form 20 bands below the Fermi level in RuS_2 in one-to-one correspondence with the occupied S $3p$ states of the hypothetical S_2^{2-} material. For future reference, we will label this group of 20 bands III and the group of 12 narrow Ru $4d$ t_{2g} bands IV. The antibonding Ru e_g-S $3p$ hybrid states form 12 bands above the Fermi level—corresponding to four bands from S $3p\sigma^*$ states and eight bands from Ru $4d$ e_g states. The group of 12 conduction bands will be labeled V. In general, the conduction-band states are strongly hybridized with each other; however, the bottom of the conduction band at Γ has pure S $3p\sigma^*$ behavior.

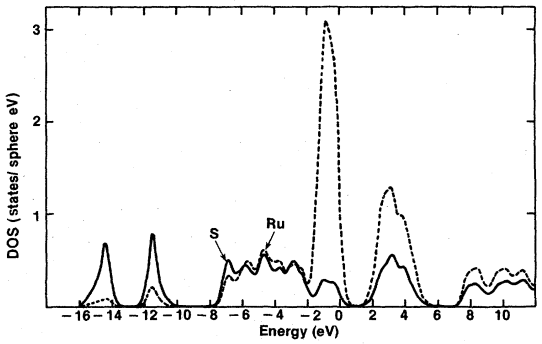

FIG. 2. Partial densities of states for pyrite RuS_2 for Ru sphere (dashed line) of radius 1.26 Å and S sphere (full line) of radius 1.09 Å. Fermi function smoothing according to Eq. (1) with $\Delta=0.15$ eV. Units for density of states include spin.

In order to further study the local bonding in RuS_2, partial densities of states were calculated as described in Sec. II. The sphere radii were chosen as 1.09 Å for S and 1.26 Å for Ru. This choice corresponds to touching spheres along the S—S molecular bond and along the nearest-neighbor S-Ru direction. The results[20] are shown in Fig. 2 using a solid line to denote the S partial density and a dashed line to denote the Ru partial density. This figure shows that there is significant hybridization between the Ru and S states, although the dominant Ru contributions are in the group-IV bands just below the Fermi level, and in the group-V bands above the Fermi level. The dominant S contributions are in the group-I and -II bands; the group-III bands having approximately equal charge in the S and Ru spheres for this choice of sphere radii. In order to study the charge contributions more quantitatively, we calculated the charge within the S and Ru spheres for each of the five groups of bands. The results are listed in Table III. This table shows that 62% of the charge within the Ru sphere is due to the group-IV ($4d$ t_{2g}) states. The charge due to $4d$ e_g states is distributed between 34% in occupied bonding group-III states and 40% in unoccupied antibonding group-V states for the Ru sphere and correspondingly 57% and 28% for the S sphere.

TABLE III. Distribution of charge in RuS_2.

	Ru sphere ($R=1.26$ Å)	S sphere ($R=1.09$ Å)
Hypothetical S_2^{2-} material		4.2 electrons
RuS_2	6.6 electrons	4.0 electrons
Partial charges in RuS_2:		
I. S $3s$ σ states (bands 1—4)	0.1 (1%)	0.7 (16%)
II. S $3s$ σ^* states (bands 5—8)	0.2 (2%)	0.7 (16%)
III. Bonding S $3p$ and Ru $4d$ e_g states (bands 9—28)	2.3 (34%)	2.3 (57%)
IV. Ru $4d$ t_{2g} states (bands 29—40)	4.1 (62%)	0.4 (10%)
V. Antibonding S $3p$ and Ru $4d$ e_g states; partial charge for bands if they were fully occupied (bands 41—52)	2.7 (40%)	1.1 (28%)

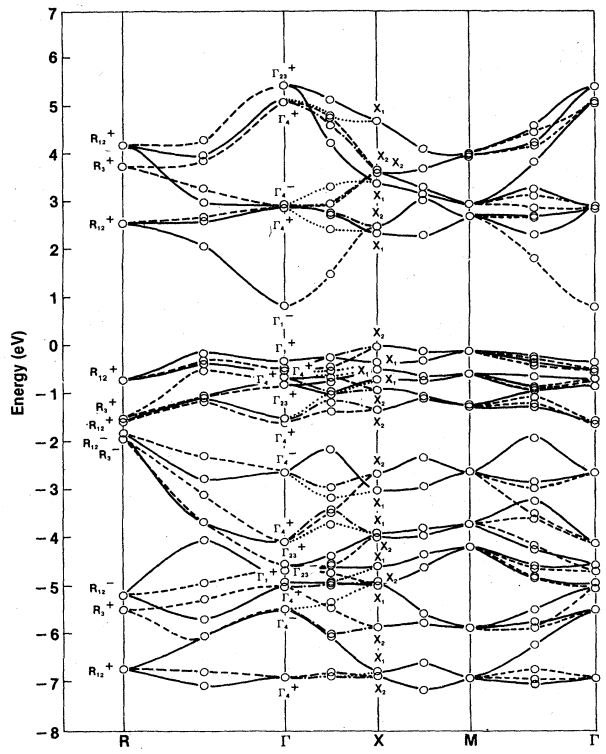

FIG. 3. Energy-band diagram for pyrite RuS_2 over portion of energy range given in Fig. 1(a). Labels for symmetry point using notation of Slater (Ref. 16). Symmetry designations along symmetry lines given with distinct line patterns as follows: R to Γ lines Λ_1 (——) and Λ_{23} (— — —); Γ to X lines Δ_1 (——), Δ_2 (— — —), Δ_3 (· · · ·), and Δ_4 (—·—·—·); M to Γ lines Σ_1 (——) and Σ_2 (— — —).

The simple molecular orbital scheme described above does a good job of explaining the basic band groupings for RuS_2. However, as recognized by several authors,[18,19] and as shown in the contour plots in Sec. III D, additional hybridizations occur. For example, since the octahedral field of the Ru sites are trigonally distorted, one would expect the t_{2g} states to be split into a singly degenerate a_1 and a doubly degenerate e state. From Figs. 1(a) and 3, it is apparent that for RuS_2, effects of the trigonal distortion are smaller than the bandwidth of the group-IV bands. As another example, since the S sites are in a nearly tetrahedral environment (trigonally distorted) due to three Ru and one S nearest neighbors, one would expect the S orbitals to have some sp^3 character. Comparing Fig. 1(a) with Fig. 1(b), where the tetrahedral field has been removed, gives some idea of this effect. It is seen as a small effect for the energy-band structure; however, the effect of S sp^3 hybridization will be seen more clearly in the charge-density plots of Sec. III D.

2. *Energy-band dispersions*

The upper part of the valence and conduction bands of RuS_2 are shown in more detail in Fig. 3. Our results indicate the RuS_2 is an indirect-gap semiconductor. The calculated indirect gap is 0.84 eV, due to the top of the valence band at X and the bottom of the conduction band at Γ, and the direct gap at the gamma point is 1.15 eV. Recent optical measurements on single crystal RuS_2 by Bichsel, Levy, and Berger[5] are consistent with an indirect gap. Their measured optical gap of 1.3 eV is larger than our calculated gap, but smaller than earlier measurements on polycrystaline samples.[21] The fact that our calculated gap is smaller than the experimental one, is a general problem associated with using local density theory for studying semiconductors and insulators. The problem stems partly from the form of the exchange-correlation approximation[22] and partly from the fact that the calculation is based on a ground-state theory and can not rigorously be used to study excited-state properties such as optical spectra.[23,24] Nevertheless, the overall features of the band structure are expected to be well represented by local density theory.[23]

The T_h^6 space group has a simple cubic unit cell for which we use the symmetry point labels of Bouckaert, Smoluchowski, and Wigner.[25] The character tables for this group have been tabulated by Slater.[16] At the Γ point, there are 24 symmetry operations. The states Γ_1^+ and Γ_1^- are each singly degenerate. The "+" and "−" symbols indicate, respectively, even and odd symmetry with respect to inversion about the center of the unit cell which we have taken to be at a Ru atom site. The Γ_2^+ and Γ_3^+ states are degenerate as are the Γ_2^- and Γ_3^- states. We have therefore used the simplified notation of Γ_{23}^+ and Γ_{23}^- to denote these pairs of levels. The Γ_4^+ and Γ_4^- states are each triply degenerate. Ru $4d$ e_g states can have Γ_4^+ or Γ_{23}^+ symmetry while Ru $4d$ t_g states can have Γ_4^+ or Γ_{23}^+ or Γ_1^+ symmetry. The R point at the corner of the Brillouin zone has 24 symmetry operations and six doubly degenerate representations. The representations R_1^+ and R_2^+ are also degenerate as are the R_1^- and R_2^- states. We use the simplified notation R_{12}^+ and R_{12}^- to denote these pairs of degenerate states. The center of a face of the Brillouin zone at X has eight symmetry operations and two sets of doubly degenerate representations. The center of an edge of the Brillouin zone at M also has eight symmetry operations and two sets of doubly degenerate representations. However, these states are also degenerate with each other.

From this symmetry analysis, we see that the indirect-band gap involves an X_2 state at the top of the valence band and a Γ_1^- state at the bottom of the conduction band. The direct-band gap involves a Γ_1^+ state at the top of the valence band and the Γ_1^- state at the bottom of the conduction band. Analysis of the optical dipole selection rules for transitions at the Γ point, shows that this direct transition is forbidden, but that transitions from energetically nearby Γ_4^+ states are allowed to the bottom of the conduction band. Since the Γ_1^- state at the bottom of the conduction band corresponds to the S $3p\sigma^*$ antibonding molecular orbital, one can infer that excitations to this state would tend to weaken the S—S bond in the pyrite structure. More generally, since the entire set of 12 conduction bands is antibonding in character, one can infer that populating these bands would tend to weaken the crystal binding. It is possible that this simple mechanism is related to the result that RuS_2 crystals suffer some

decomposition under certain photoelectrochemical conditions.[3].

In general, most of the energy-band structure of the RuS_2 is characterized by narrow bands having small dispersion. The important exception to this trend is the bottom of the Γ_1^- conduction band. A rough estimate of the effective mass of this band along the (100) direction gives a value of $0.5m_e$, suggesting that carriers in this band could have a reasonable mobility.

C. Calculated and measured densities of states for RuS_2

The total density of states for RuS_2 was calculated[20] as described in Sec. II and is shown in Fig. 4(b). The S $3s\sigma$ and σ^* bands form well-defined peaks in the density of states at -15.6 and -12.3 eV, respectively. The bonding S $3p$-Ru $4d$ e_g band has a width of 5.3 eV and a maximum energy of -1.8 eV. The Ru $4d$ t_{2g} is just below the Fermi level and has a width of 1.6 eV. The unoccupied antibonding S $3p$-Ru $4d$ e_g band has a minimum energy of 0.84 eV above E_F and has a width of 4.6 eV.

The experimental density of states as measured by angle-integrated x-ray photoemission is shown in Fig. 4(a). In these results, the experimental uncertainty in the alignment of the Fermi level is ± 0.15 eV. The strong emission peaked at -1.2 eV below the Fermi level corresponds to the Ru $4d$ t_{2g} states. In addition to these group-IV band contributions, structures due to the group-III bands are also seen at -3.2, -4.9, -5.9, and -7.4 eV. The group-I and -II bands are peaked at about -16.3 and -12.9 eV, respectively. These experimental results are similar to the XPS spectra recently published by Kuhne, Jaegermann, and Tributsch.[26] However, better resolution and lower background have been obtained in the present work.[27] In general, the agreement between experiment and calculation is very good. The agreement is least good for the group-I and -II bands for which the calculated bands are shifted to higher energy than those of the experiment by 0.7 eV. This discrepancy is due to the minimal S basis set used in these calculations; more recent calculations, including additional S s and p LCAO orbitals, shift these states closer to the experimental results. Apparent in the experimental results, and cited in the literature[18] for FeS_2, is the fact that the group-I band peak is wider than that of the group-II band peak. This trend is seen in the density of states plot, resulting from the different dispersions of the two groups of bands. In general, the results for RuS_2 are very similar to analogous results for FeS_2 both experimentally[18,28] and theoretically.[29–31]

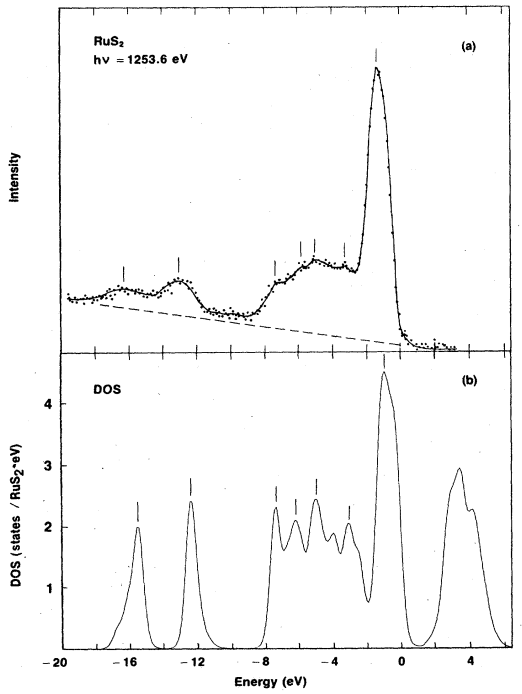

FIG. 4. (a) Experimental density of states of RuS_2 measured by x-ray photoemission. (b) Theoretical (total) density of states of RuS_2 calculated using Fermi functions smoothing according to Eq. (1) with $\Delta = 0.15$ eV. Units for density of states included spin.

D. Calculated charge densities for RuS_2

A contour plot of the self-consistent valence charge density of RuS_2 is shown in Fig. 5, in a plane containing the (110) and (100) axes. This plane was chosen because it contains the nearest-neighbor S—S bonds as well as the nearest-neighbor Ru—S bonds, exhibiting the zig-zig bonding pattern of this structure. For reference, the cube dimension a and the nearest Ru-Ru distance $a/\sqrt{2}$ is also shown in this figure. The contours associated with S are clearly shown in this figure, demonstrating both bond charge due to the S σ bonds and also π-like charge hybridizing with the Ru states. The contours associated with Ru are too dense to be clearly seen in this figure. These plots are actually plots of pseudodensity, so that the shape of the charge within the core region is smoother than the actual density. The integral of the pseudodensity within

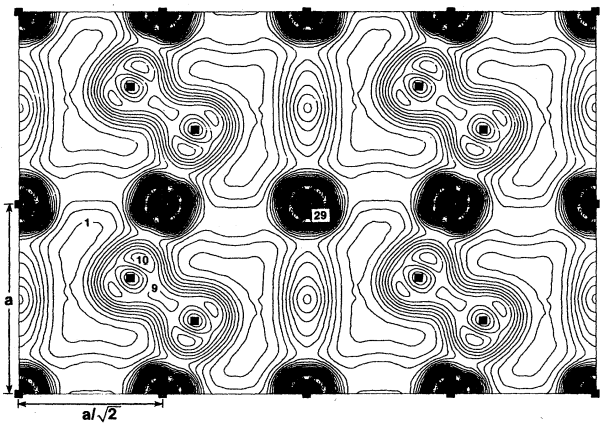

FIG. 5. Contour plot of the self-consistent valence charge density of pyrite RuS_2 in a plane containing (110) and (001) axes. Atomic positions are denoted with filled boxes. Ru sites are located in regions of dense, unresolved contour levels. Contour levels are given in units of 0.1 electrons/Å^3.

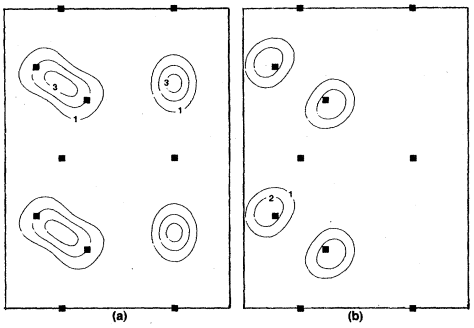

FIG. 6. Contour plot of partial self-consistent valence charge density of pyrite RuS_2 in portion of plane and using same notation as in Fig. 5: (a) I bands; (b) II bands.

the core region is the same as that of the actual density; the pseudodensity and actual density are identical in the valence region.

Figures 6 and 7 are contour plots of partial densities, plotted in a portion of the same plane as Fig. 5. Figures 6(a) and (b) show the S $3s$ σ (I) and σ^* (II) bands, respectively. Within the accuracy of the lowest contour plot, these densities appear to be of pure S character. Figures 7(a)—7(c) show the S $3p$—Ru $4d$ e_g bonding bands (III), the Ru $4d$ t_{2g} bands (IV), and the s $3p$—Ru $4d$ e_g antibonding bands (V), respectively. The bonding, nonbonding and antibonding character, respectively, of these groups of bands is clearly evident.

In Fig. 8, the total bonding density of RuS_2 (total density minus density due to t_{2g} bands) is compared with the total density of the hypothetical S_2^{2-} compound. The similarity in the S densities of the two plots is evident. This comparison can be made more accurately by taking the difference between the two densities. Figure 9(a) is the difference density from Fig. 8(a) minus Fig. 8(b). Figure

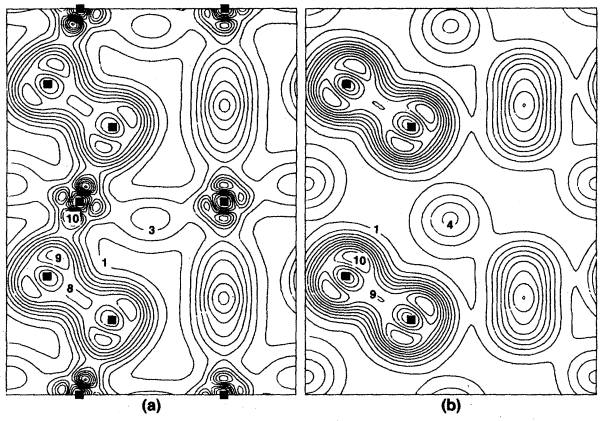

FIG. 8. Contour plot of self-consistent bonding charge density of pyrite RuS_2 (total density minus density due to group IV bands) (a), and contour plot of total self-consistent valence charge density of hypothetical S_2^{2-} material in pyrite structure (b). Portion of plane and notation is the same as for Figs. 6 and 7.

9(b) is a similar difference density based on a hypothetical neutral S_2 material. The negative contours in Fig. 9 denote regions of greater density in the hypothetical S materials than in the RuS_2 and are typically located in regions associated with S π orbitals. The positive contours denote regions of greater density in the RuS_2 than in the hypothetical S materials and are typically located in $4d$ e_g-like orbitals near the Ru sites. From Fig. 9(a), it is evident that S_2^{2-} has an excess of S $3p$ π states which are not present in RuS_2. Since the negative contours of Fig. 9(b) are of smaller magnitude than those of Fig. 9(a), one can infer that the bonding of the neutral S_2 is more similar to that of RuS_2 than is that of ionic S_2^{2-}, even though the energy-level schemes follow the opposite trend. This

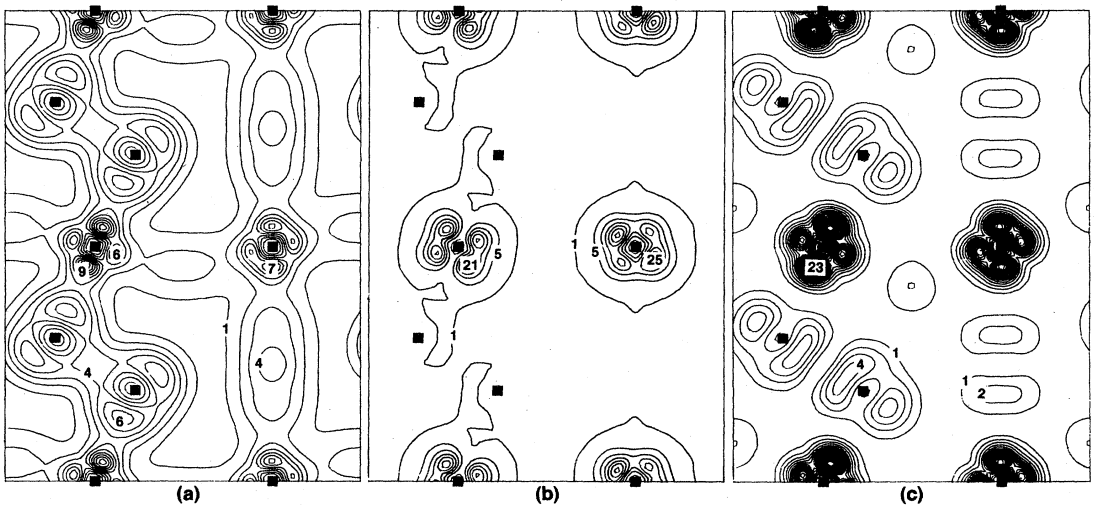

FIG. 7. Contour plot of partial self-consistent valence charge density of pyrite RuS_2 in portion of plane and using same notation as in Fig. 6: (a) III bands, (b) IV bands, and (c) V bands. In (a) and (c), contours are spaced at intervals of 0.1 electrons/Å^3; in (b) contour levels are spaced at intervals of 0.4 electrons/Å^3. In (c), the density is given as if the bands were fully occupied.

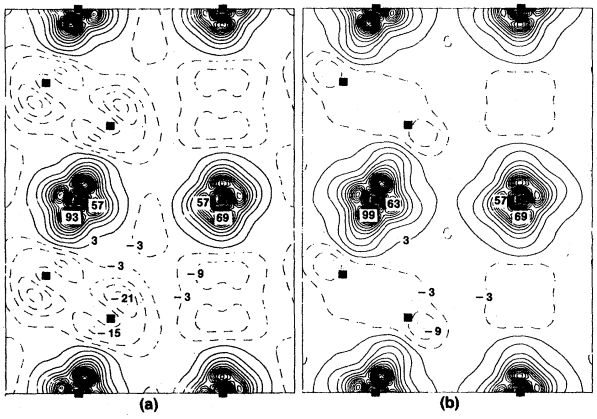

FIG. 9. Contour plot of difference density for bonding charge density of RuS_2 minus density of hypothetical S_2^{2-} material (a) and minus density of hypothetical neutral S_2 material (b). Portion of plane and notation is similar to that of previous contour plots. Negative contours are given with dashed lines, positive contours with full lines. Units of contour levels are 0.01 electrons/Å^3 and spacing between contours is 0.06 electrons/Å^3.

hybridization can most logically be described as a small admixture of S sp^3 character to the S_2 molecular orbitals as suggested by several authors.[18,19]

IV. CONCLUSIONS

In this paper we have investigated the electronic structure of RuS_2 by means of self-consistent local density calculations and x-ray photoemission. We report results for the calculated energy-band dispersions, calculated contour plot of charge densities, and calculated and measured densities of states. Our results show that the electronic structure is dominated by short-range interactions which determine the groupings of the bands. The bottom of the lowest conduction band does, however, exhibit significant dispersion.

Because of the dominance of short-range interactions, our results are similar to those published in the literature for other transition metal dichalcogenide materials. The pyrite structure materials differ from other transition metal dichalcogenides, such as those in the layered forms, due to the presence of the molecular S_2 interactions. In RuS_2 (and also FeS_2) this interaction causes the S_2 $3p\,\sigma^*$ levels to lie at higher energies that of the other S $3p$ levels, and enables the material to be a semiconductor. If these materials were to have formed in the $1T$ structure, for example, which is a structure having the same local geometry at the metal site, but having no S_2 bonds, they would probably be metallic.

We expect the present results for RuS_2 to be very similar to those for FeS_2. In a future paper, we will explore the details of this comparison. Literature results for FeS_2 (Refs. 29—31) are generally similar to the present results for RuS_2. The main qualitative difference is the relative position and dispersion of the Γ_1^- S $3p\,\sigma^*$ band.

ACKNOWLEDGMENTS

The calculations for this work were performed at Exxon Research and Engineering Company. We would like to thank Dr. R. R. Chianelli and Dr. Herbert King for helpful discussions throughout the course of this work, Dr. J. D. Passaretti for providing the RuS_2 sample, Dr. J. R. Chelikowsky for a critical reading of the manuscript, and G. J. Hughes for providing experimental help.

[1]Sutarno, O. Knop, and K. I. G. Reid, Can. J. Chem. **45**, 1391 (1967).
[2]S. Harris and R. R. Chianelli, J. Catal. **86**, 400 (1984).
[3]H. Ezzouia, R. Heindl, R. Parsons, and H. Tributsch, J. Electroanal. Chem. **165**, 155 (1984).
[4]N. A. W. Holzwarth, S. Harris, and K. S. Liang, Bull. Am. Phys. Soc. **28**, 387 (1983).
[5]R. Bichsel, F. Levy, and H. Berger, J. Phys. C **17**, L19 (1984).
[6]See, for example, J. A. Wilson and A. D. Yoffe, Adv. Phys. **18**, 193 (1969).
[7]P. Hohenberg and W. Kohn, Phys. Rev. **136**, B864 (1964); W. Kohn and L. J. Sham, *ibid.* **140**, A1133 (1965).
[8]L. Hedin and B. I. Lundqvist, J. Phys. C **4**, 2064 (1971).
[9]S. G. Louie, K.-M. Ho, and M. L. Cohen, Phys. Rev. B **19**, 1774 (1979).
[10]G. P. Kerker, J. Phys. C **13**, L189 (1980).
[11]L. Kleinman, Phys. Rev. B **21**, 2630 (1980).
[12]G. B. Bachelet and M. Schluter, Phys. Rev. B **25**, 2103 (1982).
[13]N. A. W. Holzwarth, S. G. Louie, and S. Rabii, Phys. Rev. B **26**, 5382 (1982).
[14]J. D. Passaretti, R. B. Kaner, R. Kershaw, and A. Wold, Inorg. Chem. **20**, 501 (1981).
[15]K. S. Liang, G. J. Hughes, and R. R. Chianelli J. Vac. Sci. Technol. **A2**, 991 (1984).
[16]John C. Slater, *Quantum Theory of Molecules and Solids,* (McGraw-Hill, New York, 1965), Vol. 2, Appendix 3.
[17]F. Hulliger and E. Mooser, J. Phys. Chem. Solids **26**, 429 (1965) and references cited therein.
[18]A. van der Heide, R. Hemmel, C. F. van Bruggen, and C. Haas, J. Solid State Chem. **33**, 17 (1980).
[19]J. B. Goodenough, J. Solid State Chem. **5**, 144 (1972).
[20]Note that the band "tails", especially noticeable near the Fermi level, are due to the smoothing function $f(x)$.
[21]F. Hulliger, Nature (London) **200**, 1064 (1963).
[22]Z. H. Levine and S. G. Louie, Phys. Rev. B **25**, 10 (1982).
[23]J. P. Perdew and M. Levy, Phys. Rev. Lett. **51**, 1884 (1983).
[24]L. J. Sham and M. Schluter, Phys. Rev. Lett. **51**, 1888 (1983).
[25]L. P. Bouckaert, R. Smoluchowshi, and E. Wigner, Phys. Rev. **50**, 58 (1936).
[26]H.-M. Kuhne, W. Jaegermann, and H. Tributsch, Chem. Phys. Lett. **112**, 160 (1984).
[27]K. S. Liang (unpublished).
[28]S. Suga, K. Inoue, M. Taniguchi, S. Shin, M. Seki, K. Sato, and T. Teranishi, J. Phys. Soc. Jpn. **52**, 1848 (1983).
[29]S. Asano, private communication to Suga *et al.* (Ref. 28).
[30]D. W. Bullett, J. Phys. C **15**, 6163 (1982).
[31]S. Lauer, A. X. Trautwein, and F. E. Harris, Phys. Rev. B **29**, 6774 (1984).